IMPROVING BRIGTHNESS TEMPERATURE MEASUREMENTS NEAR COASTAL AREAS

J. Chaubell[1], S. Yueh[1], J. Peng[3,4], S. Chan[1], S. Dunbar[1], D. Entekhabi[2]

[1]Jet Propulsion Laboratory, California Institute of Technology, Pasadena, CA, USA

[2]The Massachusetts Institute of Technology, Cambridge, Massachusetts, USA

[3]Goddard Space Flight Center, Greenbelt, MD, USA

[4]Universities Space Research Association, Columbia, MD, USA

ABSTRACT

The Soil Moisture Active Passive (SMAP) mission was designed to acquire and combine L-band radar and radiometer measurements for the estimation of soil moisture with 4% volumetric accuracy away from coastal zones. In regions near the coast or near inland bodies of water, the SMAP footprint contains land and water, resulting in errors in the soil moisture estimation. In this paper, we address the effort to extract the brightness temperature related to the land fraction or water fraction (depending on the center of the footprint location) from the affected SMAP measurements. We evaluate the performance of our algorithm over simulated data. We then show results over real data. The new SMAP upgraded product is expected to be delivered on April 2018.

Index Terms— SMAP, Coastal areas, Brightness temperature.

1. INTRODUCTION

The Soil Moisture Active Passive (SMAP) mission was launched on Jan 31, 2015. The mission was designed to acquire and combine L-band radar and radiometer measurements for the estimation of soil moisture with 4% volumetric accuracy (1-sigma) away from coastal zones. [1]

In regions near the coast or near inland bodies of water, the SMAP footprint contains land and water resulting in errors in the soil moisture estimation. The mixed land and water emissions lead to land brightness temperature underestimation and thus to the overestimation of soil moisture.

The determination of the land and water temperatures contributing to the sensor measurement will not only have a significant impact on the reduction of the soil moisture errors near coastal zones, but also on the retrieval of other physical parameters provided by the high level SMAP products.

Several authors have addressed the retrieval of the mixed land and water brightness temperatures using different techniques, to improve, for example, current standard Special Sensor Microwave Imager (SSM/I) products. T. Bellerby (1998) [2] used multi-pixel information to retrieve the land and sea brightness temperature by solving an overconstrained system of equations. This technique assumes the brightness temperature is constant along the area covered by the used set of measurements. Maaß and Kaleschke (2010) [3] used a single pixel technique to correct the coastal brightness temperature and the thus retrieve sea ice concentration near coastal areas in the Baltic Sea. Yang (2014) [4] compared different techniques and analyzed the sources of error of those techniques. Then, the corrected data were used for wind retrieval over the Great Lakes.

In this presented work, we apply a single measurement technique to separate the land and water contribution for the uncorrected SMAP measurements as in [3]. We summarize the methodology for the retrieval of land and water brightness temperatures (Section 2). Then we show results using simulated data (Section 3) and evaluate the performance of our approach. Finally, we show results using real data (Section 4).

2. RETRIEVAL METHODOLOGY FOR WATER AND LAND BRIGHTNESS TEMPERATURE

The brightness temperature T_B measured by the antenna can be modeled by the convolution of the antenna gain pattern with the actual distribution of brightness temperature T_b over the surface of the earth:

$$T_B(\hat{s}_0) = \frac{\int G(\hat{s}_0, \hat{s}) T_b(\hat{s}) d\Omega}{\int G(\hat{s}_0, \hat{s}) d\Omega}, \quad (1)$$

where $\hat{s}_0$ is the center of the footprint projection, and $G(\hat{s}_0, \hat{s})$ is the antenna gain pattern center at $\hat{s}_0$ and evaluated over the surface point $\hat{s}$. Equation (1) can be separated into the land and water contribution as follows:

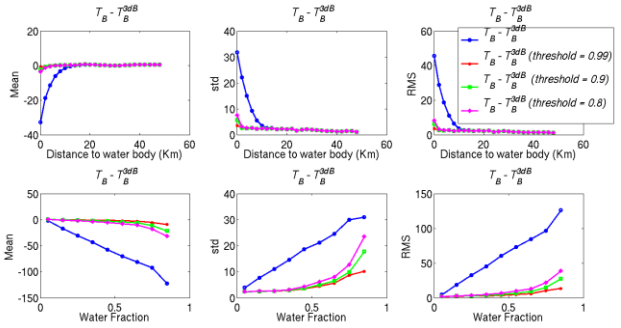

Figure 1: Mean, std, and RMSE resulting from the water contamination correction. We display the difference of uncorrected T_B - $T_{B_{land}}^{3dB}$ (blue line) and corrected T_B -$T_{B_{land}}^{3dB}$ for several thresholds (0.99, 0.9, 0.8). Top row displays statistics as a function of distance to water bodies. Bottom row displays statistics as a function of water fraction.

$$T_B(\hat{s}_0) = \frac{1}{\int G(\hat{s}_0,\hat{s})d\Omega}\left(\int G(\hat{s}_0,\hat{s})\big(1-M(\hat{s})\big)T_b(\hat{s})d\Omega + \int G(\hat{s}_0,\hat{s})M(\hat{s})T_b(\hat{s})d\Omega\right),$$

where $M(x)$ is a land mask defined over a 1Km EASE2 grid. $M(x)$=1 if x is over water and $M(x)$=0 if x is over land. Assuming that $T_b = T_B^{land}$ is constant over the land portion of the domain of integration and that $T_b = T_B^{water}$ is constant over the water portion of the domain of integration, then we have

$$T_B(\hat{s}_0) = (1-f)T_B^{land} + fT_B^{water}, \qquad (2)$$

where f is the water fraction given by

$$f = \frac{\int G(\hat{s}_0,\hat{s})M(\hat{s})d\Omega}{\int G(\hat{s}_0,\hat{s})d\Omega},$$

To retrieve the land and water brightness temperature we separate our set of measurements into two sets according to the location of the center of the antenna footprint, one for centers located over land and the other with centers located over water. We first retrieve the brightness temperature over land and then we retrieve the brightness temperature over water as follows:

1. From equation (2) replacing T_B^{water} by an estimate $\hat{T}_B^{water}$, T_B^{land} can be obtained as:

$$T_B^{land} = \frac{T_B - f\hat{T}_B^{water}}{1-f},$$

To estimate the brightness temperature over water, $\hat{T}_B^{water}$,we search for measurements with the footprint center located over water and with a water fraction greater than a pre-fixed threshold to assure the selection of contamination-free measurements. The extent of the searching region is also pre-fixed to assure that we can find measurements within it. If measurements satisfying the threshold condition are not found within the region then a default value is used. The default value is either the average of all the

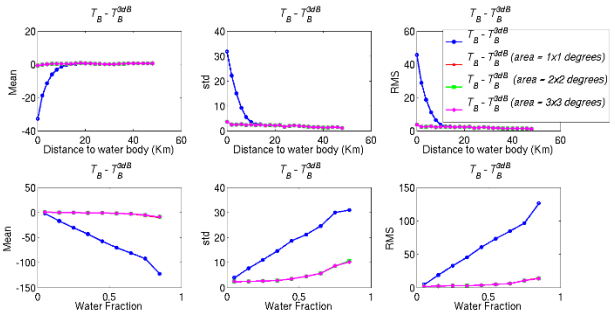

Figure 2: Mean, std, and RMSE resulting from the water contamination correction. We display the difference of uncorrected T_B - $T_{B_{land}}^{3dB}$ (blue line) and corrected T_B -$T_{B_{land}}^{3dB}$ for several searching areas (1x1 degrees, 2x2 degrees and 3x3 degrees). Top row displays statistics as a function of distance to water bodies. Bottom row displays statistics as a function of water fraction.

measurements on the half-orbit pass satisfying the threshold condition or the previously selected water brightness temperature.

2. From equation (2) replacing T_B^{land} by an estimate $\hat{T}_B^{land}$, T_B^{water} can be obtained as:

$$T_B^{water} = \frac{T_B - (1-f)\hat{T}_B^{land}}{f},$$

The estimation of the land temperature following a similar algorithm, as in item 1, is challenging due to the greater variance of the land temperatures. In addition, searching for measurements free of contamination requires looking into regions away from the coastal zones leading to averaged temperatures that might not be representative of the real coastal brightness temperature. Therefore, we apply an alternative method by modifying our algorithm to mitigate those challenges. Taking advantage of the already corrected land temperatures, as in item 1, we can reduce the searching area and allow for the selection of corrected temperatures closer to the coastal zone without imposing water fraction conditions (these measurements are no longer affected by contamination). Then we obtain the inverse distance weighted average temperature from temperatures already free of contamination.

Note that to avoid division for numbers close to zero we retrieve land brightness temperatures for measurements with water fraction smaller than 0.9 and we retrieve the water brightness temperatures with water fraction greater than 0.1.

3. SIMULATED DATA AND RETRIVAL RESULTS

Our simulated SMAP measurement of the brightness temperature T_B follows equation (1), ignoring atmospheric and galactic effects. The emitted brightness temperature T_b over land surface is computed using a plane surface model taking into account the surface temperature, the frequency (1.414 GHz), the incidence angle (~40 degrees) and the dielectric constant which is computed using the Mironov's model [5]. Our land dielectric constant takes into account soil moisture content and clay fraction only (bare

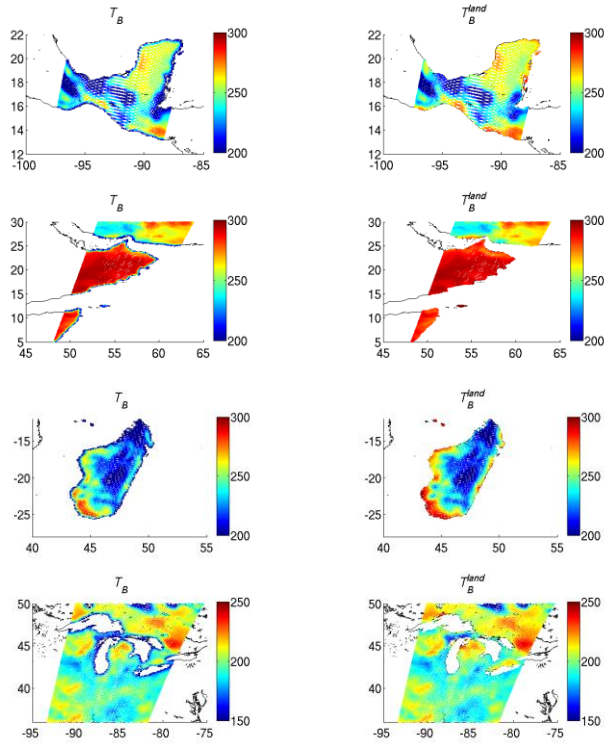

Figure 3: Results obtained using simulated data. Left: The SMAP simulated measurements before correction. Right: Corrected land brightness temperatures. From top to bottom we have: a) Madagascar, b) Great Lakes, c) Yucatan Peninsula, d) Arabian Sea.

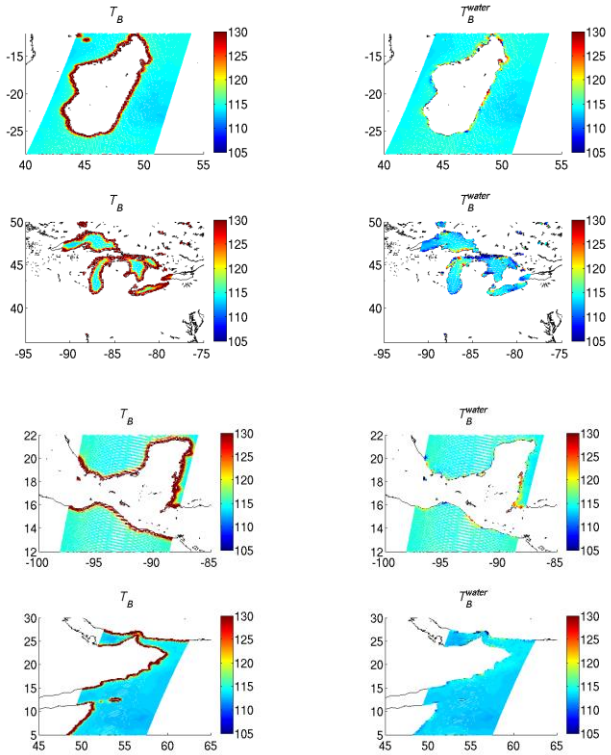

Figure 4: Results obtained using simulated data. Left: The SMAP simulated measurements before correction. Right: Corrected water brightness temperatures. From top to bottom, we have a) Madagascar, b) Great Lakes, c) Yucatan Peninsula, d) Arabian Sea.

soil). The model for the T_b over water follows the model presented by Yueh (2012) [6]. This model takes into account wind, sea surface temperature, and salinity.

To evaluate the performance of our algorithm to retrieve brightness temperature over land, we compare the uncorrected and corrected brightness temperature against the simulated brightness temperature contribution over the 3dB beam coming from land only

$$T_{B_{land}}^{3dB}(\hat{s}_0) = \frac{\int G(\hat{s}_0,\hat{s})(1-M(\hat{s}))T_b(\hat{s})d\Omega_{3dB}}{\int G(\hat{s}_0,\hat{s})d\Omega_{3dB}},$$

where Ω_{3dB} is the 3dB beam domain of integration.

The T_B and $T_{B_{land}}^{3dB}$ were simulated for different earth regions and then the corrected T_B^{land} was computed as it was stated in the previous section in item 1. The uncorrected T_B and the corrected T_B^{land} were compared against $T_{B_{land}}^{3dB}$. Before applying our algorithm, two parameters (water fraction threshold and the dimensions of the searching area) need to be set in order to estimate $\hat{T}_B^{water}$. Figure 1 displays the mean, standard deviation (std) and the root mean square (RMS) of the differences, $(T_B - T_{B_{land}}^{3dB})$, as a function of distance to water bodies (top row) and as a function of water fraction (bottom row) for different thresholds values. To evaluate the statistics as a function of distance to water bodies, we binned the data into 2km bins and then the mean, std and RMS of differences were evaluated for each bin. To evaluate the statistics as a function of water fraction the data were binned into 0.1 water fraction increments. Those results show that the performance improves when the threshold gets closer to one (red line). We also observe that the performance deteriorates as the water fraction tends to one (footprint on small pieces of land surrounded by water). Figure 2 displays the statistics from results obtained for different searching area dimensions showing that the size of the area does not affect the incoming results. Thus, based on our sensitivity results we set the water fraction threshold to 0.99 and the searching area dimension to 3x3 degrees in a latitude and longitude to assure we have enough measurements within the area under consideration satisfying the threshold condition. Figure 3 displays maps of the uncorrected land T_B (left) and the corrected T_B^{land} for several regions. We can notice that the smooth transition between land and water was eliminated after correction creating sharper edges.

We then retrieve T_B^{water} as stated in item 2 of the previous section and we compare it against the corresponding 3 dB brightness temperature contribution from water given by

$$T_{B_{water}}^{3dB}(\hat{s}_0) = \frac{\int G(\hat{s}_0,\hat{s})M(\hat{s})T_b(\hat{s})d\Omega_{3dB}}{\int G(\hat{s}_0,\hat{s})d\Omega_{3dB}}.$$

The searching area for the estimation of $\hat{T}_B^{land}$ was set to 1x1 degree in latitude and longitude and the alternative method was applied. Maps of uncorrected water T_B and corrected T_B^{water} are displayed in Figure 4. We can see how the dark edges on the left column maps disappear after correction.

4. REAL DATA RESULTS

The results over real data were obtained following the same algorithm described in the previous section. We should not expect the same performance obtained with simulated data due to the presence of other sources of errors when dealing with real data such as geolocation errors, greater variability of brightness temperature (vegetation, urban areas…), etc. Maps showing results using real data are displayed in Figure 5 and Figure 6. In Figure 5 we can observe that the intense blue borders corresponding to cold temperatures in the coastal areas were removed after correction. Figure 6 shows the uncorrected and corrected brightness temperature over ocean. We can see in some areas that the corrected brightness temperatures over ocean are underestimated. We suspect that residual pointing errors maybe the cause of those anomalies but the problem is still being investigated.

5. CONCLUSION

An algorithm to improve the brightness temperature measurements over coastal areas and near bodies of water was implemented. Overall, our algorithm performed very well. Results over simulated data show significant statistical improvements. Results over real data show that our algorithm eliminates the cold borders over land and the warmer borders over ocean. Some anomalies, however, are still being investigated.

6. ACKNOWLEDGMENT

This work is carried out by the Jet Propulsion Laboratory, California Institute of Technology, under a contract with the National Aeronautics and Space Administration.

7. REFERENCE

[1] D. Entekhabi et al. “The Soil Moisture Active Passive (SMAP) Mission,” Proceedings of the IEEE, vol. 98, no. 5, pp. 704-716, May 2010.

[2] T. Bellerby, M. Taberner, A. Wilmshurst, M. Beaumont, E. Barrett, C. Durbin, and J. Scott, “Retrieval of land and sea brightness temperatures from mixed pixels in coastal passive microwave data,” *IEEE Trans. Geosci. Remote Sensing*, vol. 36, pp. 1844–1851, 1998.

[3] Maaß, N., and L. Kaleschke, 2010: Improving passive microwave sea ice concentration algorithms for coastal areas: Applications to the Baltic Sea. Tellus, 62A, 393–410, doi:10.1111/j.1600-0870.2010.00452.x.

[4] Yang, J.X.; Mckague, D.S.; Ruf, C.S. Land contamination correction for passive microwave radiometer data: Demonstration of wind retrieval in the Great Lakes using SSM/I. J. Atmos. Ocean. Technol. **2014**, 31, 2094–2113.

[5] Mironov, V. L., L. G. Kosolapova, and S. V. Fomin, \Soil dielectric model accounting for contribution of bound water spectra through clay content," *PIERS Online*, Vol. 4, No. 1, 31{35, 2008.

[6] S. Yueh and J. Chaubell, “Sea surface salinity and wind retrieval using combined passive and active L-band microwave observations,” *IEEE Trans. Geosci. Remote Sens.*, vol. 50, no. 4, pp. 1022–1032, Apr. 2012.

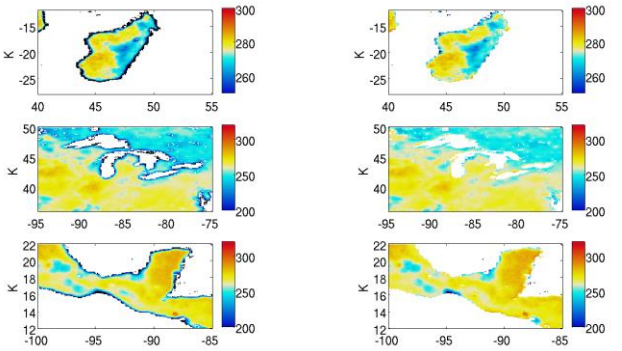

Figure 5: Results over land using real SMAP measurements. Left: uncorrected data. Right: corrected land brightness temperature.

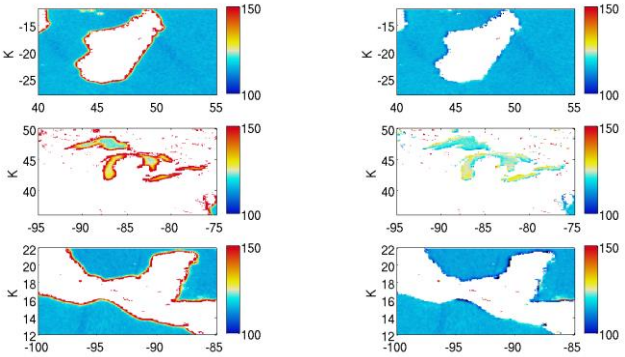

Figure 6: Results over land using real SMAP measurements. Left: uncorrected data. Right: corrected water brightness temperature.